

Supplement of Atmos. Chem. Phys. Discuss., 15, 11369–11407, 2015
<http://www.atmos-chem-phys-discuss.net/15/11369/2015/>
doi:10.5194/acpd-15-11369-2015-supplement
© Author(s) 2015. CC Attribution 3.0 License.



Supplement of

Use of North American and European air quality networks to evaluate global chemistry-climate modeling of surface ozone

J. L. Schnell et al.

Correspondence to: J. L. Schnell (jschnell@uci.edu)

Table S1. Longitude range for each latitude range used in the interpolation over NA and EU.

| <i>North America (NA)^a</i> | | <i>Europe (EU)^b</i> | |
|--|--|--|--|
| Latitude range (°N, southern- northern edge) | Longitude range (°E, western-eastern edge) | Latitude range (°N, southern- northern edge) | Longitude range (°E, western-eastern edge) |
| 25-26 | 278-280 | 36-37 | 352-358 |
| 26-27 | 260-263; 277-280 | 37-38 | 351-360; 12-17; 21-24 |
| 27-28 | 260-263; 277-280 | 38-39 | 350-1; 8-24 |
| 28-29 | 259-265; 277-280 | 39-40 | 350-1; 8-24 |
| 29-30 | 255-280 | 40-41 | 351-2; 8-24; 26-29 |
| 30-31 | 254-280 | 41-42 | 351-3; 8-30 |
| 31-32 | 247-280 | 42-43 | 350-3; 8-29 |
| 32-33 | 242-281 | 43-44 | 350-29 |
| 33-34 | 241-282 | 44-45 | 355-30 |
| 34-35 | 239-284 | 45-46 | 355-31 |
| 35-36 | 238-285 | 46-47 | 355-31 |
| 36-37 | 238-285 | 47-48 | 355-31 |
| 37-38 | 237-285 | 48-49 | 355-30 |
| 38-39 | 236-285 | 49-50 | 354-29 |
| 39-40 | 236-286 | 50-51 | 354-28 |
| 40-41 | 235-288 | 51-52 | 349-28 |
| 41-42 | 235-290 | 52-53 | 349-28 |
| 42-43 | 235-290 | 53-54 | 349-29 |
| 43-44 | 235-292 | 54-55 | 349-29 |
| 44-45 | 235-293 | 55-56 | 351-30 |
| 45-46 | 235-293 | 56-57 | 352-31 |
| 46-47 | 235-293 | 57-58 | 352-31 |
| 47-48 | 235-293 | 58-59 | 353-32 |
| 48-49 | 235-293 | 59-60 | 356-33 |
| | | 60-61 | 357-33 |
| | | 61-62 | 4-33 |
| | | 62-63 | 5-33 |
| | | 63-64 | 7-34 |
| | | 64-65 | 11-32 |
| | | 65-66 | 12-32 |
| | | 66-67 | 13-32 |
| | | 67-68 | 17-32 |
| | | 68-69 | 18-32 |
| | | 69-70 | 20-31 |
| | | 70-71 | 23-28 |

^aWestern (WNA) and eastern (ENA) North America is split by 264°E

^bSouthern (SEU) and northern (NEU) Europe is split by 53°N

Table S2. Summary statistics for the observations (OBS), ACCMIP models (A-H), and UCI CTM (I) with respect to summer (JJA) and winter (DJF) diurnal cycles.

| Data | Metric, description (unit) | OBS | A | B | C | D | E | F | G | H | I |
|--------------------------|------------------------------------|------|------|-------|------|------|------|------|------|------|------|
| WNA diurnal summer (JJA) | h , maximum phase (hour) | 15.3 | 16.6 | 16.6 | 16.5 | 15.4 | 15.3 | 14.9 | 15.2 | 16.0 | 12.9 |
| | H , peak-to-peak amplitude (ppb) | 26.8 | 28.4 | 17.7 | 20.3 | 22.8 | 20.6 | 18.1 | 11.5 | 17.9 | 34.4 |
| | MB, mean bias (ppb) | - | 3.6 | 10.8 | -0.5 | 5.1 | 2.4 | 4.6 | 5.9 | 14.7 | 20.0 |
| | R , cycle correlation | 1.00 | 0.92 | 0.92 | 0.94 | 0.99 | 1.00 | 0.98 | 0.99 | 0.97 | 0.75 |
| | NSD, normalized standard deviation | 1.00 | 1.07 | 0.69 | 0.75 | 0.84 | 0.76 | 0.67 | 0.43 | 0.69 | 1.33 |
| ENA diurnal summer (JJA) | h , maximum phase (hour) | 15.0 | 17.0 | 16.1 | 16.5 | 15.5 | 15.8 | 15.2 | 15.7 | 16.0 | 12.7 |
| | H , peak-to-peak amplitude (ppb) | 29.1 | 28.3 | 28.4 | 21.8 | 22.7 | 21.8 | 22.6 | 12.1 | 18.5 | 54.0 |
| | MB, mean bias (ppb) | - | 19.0 | 24.4 | 1.1 | 12.2 | 3.5 | 17.9 | 21.1 | 12.9 | 37.0 |
| | R , cycle correlation | 1.00 | 0.87 | 0.95 | 0.92 | 0.99 | 0.97 | 0.98 | 0.96 | 0.95 | 0.75 |
| | NSD, normalized standard deviation | 1.00 | 0.99 | 0.99 | 0.74 | 0.78 | 0.75 | 0.77 | 0.44 | 0.66 | 1.95 |
| SEU diurnal summer (JJA) | h , maximum phase (hour) | 15.5 | 16.4 | 16.6 | 16.4 | 15.1 | 15.6 | 15.3 | 15.5 | 16.3 | 13.1 |
| | H , peak-to-peak amplitude (ppb) | 24.3 | 31.9 | 20.3 | 18.8 | 21.3 | 16.2 | 15.0 | 12.9 | 15.3 | 36.0 |
| | MB, mean bias (ppb) | - | 17.0 | 17.8 | 5.2 | 16.8 | 1.0 | 12.4 | 21.8 | 14.3 | 31.5 |
| | R , cycle correlation | 1.00 | 0.96 | 0.94 | 0.97 | 0.99 | 1.00 | 0.99 | 0.99 | 0.97 | 0.74 |
| | NSD, normalized standard deviation | 1.00 | 1.33 | 0.87 | 0.77 | 0.87 | 0.67 | 0.62 | 0.54 | 0.65 | 1.54 |
| NEU diurnal summer (JJA) | h , maximum phase (hour) | 15.1 | 17.1 | 16.7 | 16.5 | 15.0 | 16.0 | 15.6 | 16.2 | 15.8 | 14.4 |
| | H , peak-to-peak amplitude (ppb) | 13.9 | 15.8 | 11.2 | 10.0 | 11.1 | 8.2 | 9.0 | 7.2 | 8.7 | 13.1 |
| | MB, mean bias (ppb) | - | 15.9 | 11.2 | 4.9 | 13.8 | 0.9 | 8.8 | 12.7 | 3.7 | 23.5 |
| | R , cycle correlation | 1.00 | 0.86 | 0.90 | 0.93 | 1.00 | 0.96 | 0.99 | 0.94 | 0.97 | 0.97 |
| | NSD, normalized standard deviation | 1.00 | 1.16 | 0.82 | 0.72 | 0.80 | 0.59 | 0.65 | 0.53 | 0.64 | 0.95 |
| WNA diurnal winter (DJF) | h , maximum phase (hour) | 14.8 | 17.1 | 17.9 | 16.0 | 14.8 | 15.0 | 15.6 | 14.0 | 16.8 | 16.7 |
| | H , peak-to-peak amplitude (ppb) | 9.8 | 11.5 | 5.9 | 8.8 | 7.5 | 6.2 | 7.9 | 3.7 | 6.0 | 13.2 |
| | MB, mean bias (ppb) | - | 6.4 | 16.7 | 14.4 | 6.8 | 2.0 | 6.1 | 23.6 | 13.6 | 8.2 |
| | R , cycle correlation | 1.00 | 0.76 | 0.69 | 0.92 | 0.98 | 0.97 | 0.95 | 0.95 | 0.88 | 0.83 |
| | NSD, normalized standard deviation | 1.00 | 1.06 | 0.54 | 0.80 | 0.69 | 0.58 | 0.73 | 0.35 | 0.60 | 1.18 |
| ENA diurnal winter (DJF) | h , maximum phase (hour) | 15.1 | 18.0 | 16.7 | 15.7 | 15.3 | 14.0 | 15.9 | 14.8 | 16.3 | 16.1 |
| | H , peak-to-peak amplitude (ppb) | 9.1 | 6.7 | 7.5 | 11.3 | 7.8 | 5.8 | 6.9 | 2.4 | 10.6 | 12.6 |
| | MB, mean bias (ppb) | - | 10.2 | 13.2 | 9.8 | -1.5 | -4.6 | 4.0 | 30.1 | 5.5 | 4.8 |
| | R , cycle correlation | 1.00 | 0.72 | 0.90 | 0.98 | 0.99 | 0.92 | 0.97 | 0.97 | 0.95 | 0.92 |
| | NSD, normalized standard deviation | 1.00 | 0.72 | 0.76 | 1.16 | 0.82 | 0.61 | 0.71 | 0.25 | 1.12 | 1.26 |
| SEU diurnal winter (DJF) | h , maximum phase (hour) | 15.1 | 17.6 | 17.8 | 16.1 | 15.0 | 14.2 | 15.8 | 14.7 | 16.4 | 16.4 |
| | H , peak-to-peak amplitude (ppb) | 5.1 | 3.5 | 3.5 | 6.7 | 4.2 | 2.5 | 3.9 | 1.4 | 5.1 | 10.8 |
| | MB, mean bias (ppb) | - | 8.3 | 17.5 | 18.4 | 8.6 | 5.7 | 9.6 | 27.7 | 12.5 | 12.7 |
| | R , cycle correlation | 1.00 | 0.71 | 0.71 | 0.90 | 0.93 | 0.86 | 0.91 | 0.95 | 0.91 | 0.82 |
| | NSD, normalized standard deviation | 1.00 | 0.95 | 0.53 | 1.04 | 0.67 | 0.41 | 0.60 | 0.23 | 0.83 | 1.63 |
| NEU diurnal winter (DJF) | h , maximum phase (hour) | 4.5 | 17.8 | 6.5 | 14.9 | 14.5 | 13.3 | 15.3 | 12.2 | 15.0 | 16.2 |
| | H , peak-to-peak amplitude (ppb) | 0.2 | 1.5 | 0.2 | 1.5 | 1.1 | 0.9 | 0.8 | 0.4 | 1.5 | 2.4 |
| | MB, mean bias (ppb) | - | -2.7 | 13.8 | 15.4 | 2.3 | -1.4 | 0.0 | 26.9 | 6.2 | 8.2 |
| | R , cycle correlation | 1.00 | 0.27 | -0.72 | 0.50 | 0.54 | 0.27 | 0.40 | 0.24 | 0.45 | 0.32 |
| | NSD, normalized standard deviation | 1.00 | 1.01 | 0.27 | 1.06 | 0.83 | 0.63 | 0.52 | 0.28 | 1.05 | 1.56 |

Table S3. Summary statistics for the observations (OBS), ACCMIP models (A-H), and UCI CTM (I) with respect to the annual cycle of MDA8.

| Data | Metric, description (unit) | OBS | A | B | C | D | E | F | G | H | I |
|-----------------------|---|------|------|------|-------|------|------|------|-------|------|------|
| WNA annual MDA8 | m , maximum phase (month) | 5.6 | 5.5 | 4.9 | 3.3 | 5.4 | 5.6 | 5.6 | 1.5 | 6.6 | 6.0 |
| | M , peak-to-peak amplitude (ppb) | 21.7 | 16.7 | 13.0 | 12.4 | 20.4 | 20.6 | 15.9 | 5.0 | 18.3 | 37.0 |
| | MB, mean bias (ppb) | - | 6.9 | 10.6 | 6.9 | 4.7 | -0.5 | 2.4 | 10.0 | 10.6 | 15.5 |
| | R , cycle correlation | 1.00 | 0.96 | 0.90 | 0.36 | 0.98 | 1.00 | 0.99 | -0.49 | 0.86 | 0.97 |
| | NSD, normalized standard deviation | 1.00 | 0.82 | 0.66 | 0.68 | 0.94 | 0.94 | 0.74 | 0.24 | 0.88 | 1.71 |
| | \bar{E}_{JJA} , 87th – 30th percentile (ppb) | 19.7 | 19.5 | 14.5 | 16.4 | 17.9 | 17.2 | 15.1 | 17.5 | 18.5 | 29.7 |
| | R_{E-JJA} , spatial correlation of E_{JJA} maps | 1.00 | 0.54 | 0.59 | 0.28 | 0.43 | 0.47 | 0.59 | 0.17 | 0.61 | 0.63 |
| ENA annual MDA8 | m , maximum phase (month) | 5.3 | 5.8 | 6.0 | 3.7 | 5.8 | 5.7 | 6.1 | 6.0 | 6.2 | 6.3 |
| | M , peak-to-peak amplitude (ppb) | 20.7 | 29.8 | 29.1 | 12.8 | 32.7 | 25.9 | 31.5 | 3.5 | 20.3 | 64.6 |
| | MB, mean bias (ppb) | - | 16.9 | 16.6 | 6.8 | 4.2 | -4.2 | 8.1 | 20.1 | 8.0 | 24.8 |
| | R , cycle correlation | 1.00 | 0.95 | 0.90 | 0.57 | 0.96 | 0.96 | 0.93 | 0.56 | 0.89 | 0.86 |
| | NSD, normalized standard deviation | 1.00 | 1.47 | 1.45 | 0.83 | 1.57 | 1.24 | 1.51 | 0.28 | 1.03 | 3.08 |
| | \bar{E}_{JJA} , 87th – 30th percentile (ppb) | 22.8 | 33.0 | 27.5 | 19.4 | 27.0 | 22.4 | 28.3 | 19.1 | 21.9 | 56.1 |
| | R_{E-JJA} , spatial correlation of E_{JJA} maps | 1.00 | 0.70 | 0.81 | 0.52 | 0.69 | 0.69 | 0.34 | 0.27 | 0.69 | 0.71 |
| SEU annual MDA8 | m , maximum phase (month) | 5.5 | 5.8 | 5.6 | 4.0 | 5.8 | 5.5 | 5.7 | 6.7 | 6.2 | 5.9 |
| | M , peak-to-peak amplitude (ppb) | 26.3 | 37.9 | 22.7 | 14.6 | 33.8 | 17.4 | 24.9 | 11.9 | 21.0 | 49.4 |
| | MB, mean bias (ppb) | - | 15.6 | 16.2 | 13.0 | 11.4 | 1.3 | 8.1 | 21.1 | 11.2 | 23.7 |
| | R , cycle correlation | 1.00 | 0.98 | 1.00 | 0.66 | 0.98 | 0.99 | 0.97 | 0.78 | 0.91 | 0.97 |
| | NSD, normalized standard deviation | 1.00 | 1.45 | 0.86 | 0.64 | 1.27 | 0.66 | 0.94 | 0.49 | 0.84 | 1.87 |
| | \bar{E}_{JJA} , 87th – 30th percentile (ppb) | 23.6 | 30.1 | 18.0 | 16.7 | 24.9 | 15.2 | 20.9 | 14.8 | 18.8 | 37.9 |
| | R_{E-JJA} , spatial correlation of E_{JJA} maps | 1.00 | 0.33 | 0.71 | 0.15 | 0.77 | 0.54 | 0.46 | 0.24 | 0.65 | 0.62 |
| NEU annual MDA8 | m , maximum phase (month) | 4.3 | 5.6 | 3.9 | 2.7 | 5.5 | 4.7 | 5.4 | 1.1 | 3.9 | 5.6 |
| | M , peak-to-peak amplitude (ppb) | 17.4 | 32.8 | 14.0 | 18.3 | 22.7 | 12.4 | 19.3 | 10.4 | 8.3 | 26.2 |
| | MB, mean bias (ppb) | - | 8.3 | 12.2 | 11.8 | 7.0 | -2.0 | 2.1 | 19.1 | 4.6 | 15.1 |
| | R , cycle correlation | 1.00 | 0.78 | 0.97 | 0.64 | 0.82 | 0.96 | 0.82 | 0.00 | 0.88 | 0.78 |
| | NSD, normalized standard deviation | 1.00 | 1.87 | 0.82 | 1.21 | 1.29 | 0.71 | 1.09 | 0.67 | 0.57 | 1.48 |
| | \bar{E}_{JJA} , 87th – 30th percentile (ppb) | 15.8 | 30.5 | 15.3 | 19.5 | 17.7 | 13.4 | 17.6 | 14.4 | 13.3 | 20.9 |
| | R_{E-JJA} , spatial correlation of E_{JJA} maps | 1.00 | 0.51 | 0.50 | -0.39 | 0.63 | 0.63 | 0.66 | 0.11 | 0.23 | 0.63 |

Table S4. Summary statistics for the observations (OBS), ACCMIP models (A-H), and UCI CTM (I) with respect to the annual cycle of AQX events and AQX episodes (NA and EU combined, 100 AQX events per decade case).

| Data | Metric, description (unit) | OBS | A | B | C | D | E | F | G | H | I |
|-----------------------|--|------|------|------|-------|------|------|------|-------|------|------|
| WNA AQX events | m_{AOX} , maximum phase (month) | 6.1 | 5.9 | 4.6 | 3.0 | 4.9 | 6.0 | 6.1 | 1.7 | 7.5 | 6.5 |
| | R , AQX cycle correlation | 1.00 | 0.85 | 0.41 | -0.24 | 0.57 | 0.97 | 0.96 | -0.07 | 0.64 | 0.78 |
| | NSD, normalized standard deviation | 1.00 | 0.53 | 0.65 | 1.74 | 1.15 | 1.01 | 1.06 | 0.57 | 1.35 | 1.58 |
| | R_{MDA8} , correlation of AQX and MDA8 cycles | 0.81 | 0.82 | 0.89 | 0.91 | 0.80 | 0.82 | 0.77 | 0.59 | 0.78 | 0.69 |
| | \bar{E}_{AOX} , AQX threshold – 30th percentile (ppb) | 27.6 | 29.2 | 20.6 | 26.9 | 24.4 | 23.7 | 21.5 | 25.4 | 26.7 | 43.2 |
| | R_{E-AOX} , spatial correlation of E_{AOX} maps | 1.00 | 0.66 | 0.66 | 0.40 | 0.49 | 0.35 | 0.56 | 0.36 | 0.55 | 0.62 |
| ENA AQX events | m_{AOX} , maximum phase (month) | 5.5 | 6.2 | 6.8 | 3.2 | 6.2 | 6.4 | 6.6 | 6.8 | 7.7 | 6.6 |
| | R , AQX cycle correlation | 1.00 | 0.80 | 0.65 | 0.04 | 0.88 | 0.79 | 0.76 | 0.70 | 0.36 | 0.65 |
| | NSD, normalized standard deviation | 1.00 | 1.11 | 1.44 | 1.90 | 1.22 | 1.27 | 1.29 | 1.03 | 1.25 | 1.48 |
| | R_{MDA8} , correlation of AQX and MDA8 cycles | 0.84 | 0.76 | 0.78 | 0.88 | 0.78 | 0.82 | 0.80 | 0.78 | 0.70 | 0.83 |
| | \bar{E}_{AOX} , AQX threshold – 30th percentile (ppb) | 34.7 | 53.8 | 39.9 | 29.1 | 36.1 | 30.4 | 41.1 | 32.1 | 31.5 | 82.3 |
| | R_{E-AOX} , spatial correlation of E_{AOX} maps | 1.00 | 0.70 | 0.78 | 0.28 | 0.63 | 0.53 | 0.44 | 0.60 | 0.74 | 0.68 |
| SEU AQX events | m_{AOX} , maximum phase (month) | 6.0 | 6.2 | 6.0 | 3.2 | 5.8 | 5.8 | 6.0 | 6.8 | 7.3 | 6.3 |
| | R , AQX cycle correlation | 1.00 | 0.97 | 0.96 | -0.09 | 0.88 | 0.96 | 0.93 | 0.78 | 0.64 | 0.90 |
| | NSD, normalized standard deviation | 1.00 | 0.99 | 1.11 | 1.68 | 1.30 | 0.96 | 1.19 | 1.17 | 1.40 | 1.33 |
| | R_{MDA8} , correlation of AQX and MDA8 cycles | 0.81 | 0.79 | 0.76 | 0.84 | 0.73 | 0.84 | 0.82 | 0.90 | 0.74 | 0.80 |
| | \bar{E}_{AOX} , AQX threshold – 30th percentile (ppb) | 33.9 | 46.3 | 24.3 | 25.1 | 30.8 | 21.5 | 30.2 | 26.3 | 29.3 | 57.4 |
| | R_{E-AOX} , spatial correlation of E_{AOX} maps | 1.00 | 0.33 | 0.70 | 0.12 | 0.66 | 0.42 | 0.20 | 0.07 | 0.58 | 0.51 |
| NEU AQX events | m_{AOX} , maximum phase (month) | 4.3 | 5.5 | 3.9 | 3.2 | 5.3 | 4.6 | 5.6 | 4.2 | 4.4 | 5.9 |
| | R , cycle correlation | 1.00 | 0.46 | 0.84 | 0.67 | 0.46 | 0.86 | 0.46 | 0.19 | 0.98 | 0.29 |
| | NSD, normalized standard deviation | 1.00 | 0.81 | 0.85 | 1.57 | 1.18 | 0.88 | 0.99 | 0.91 | 0.74 | 1.14 |
| | R_{MDA8} , correlation of AQX and MDA8 cycles | 0.87 | 0.84 | 0.93 | 0.85 | 0.73 | 0.93 | 0.85 | 0.26 | 0.90 | 0.74 |
| | \bar{E}_{AOX} , AQX threshold – 30th percentile (ppb) | 23.9 | 45.8 | 20.6 | 29.1 | 23.3 | 19.5 | 29.1 | 21.8 | 17.9 | 31.6 |
| | R_{E-AOX} , spatial correlation of E_{AOX} maps | 1.00 | 0.51 | 0.55 | -0.47 | 0.54 | 0.53 | 0.55 | 0.53 | 0.45 | 0.60 |
| NA AQX episodes | \bar{S} , weighted geometric mean AQX episode size (10^4 km ² -days) | 415 | 128 | 229 | 1426 | 461 | 290 | 522 | 243 | 774 | 463 |
| | CCD_{100} , fraction of AQX events' areas in AQX episodes > 100×10^4 km ² -days (%) | 79.0 | 56.1 | 73.7 | 92.6 | 85.3 | 76.1 | 80.3 | 73.0 | 83.0 | 80.2 |
| | CCD_{1000} , fraction of AQX events' area in AQX episodes > 1000×10^4 km ² -days (%) | 38.0 | 9.7 | 12.8 | 69.2 | 30.8 | 19.2 | 43.6 | 12.7 | 48.7 | 37.5 |
| | $\Delta \bar{E}_S$, average increase in E_S for AQX episodes of size S (ppb-dec ⁻¹) | 2.9 | 9.9 | 4.6 | 0.8 | 2.3 | 2.9 | -0.1 | 3.5 | 2.9 | 6.0 |
| EU AQX episodes | \bar{S} , weighted geometric mean AQX episode size (10^4 km ² -days) | 444 | 173 | 198 | 2106 | 656 | 290 | 616 | 498 | 606 | 535 |
| | CCD_{100} , fraction of AQX events' areas in AQX episodes > 100×10^4 km ² -days (%) | 80.1 | 63.1 | 70.6 | 92.8 | 82.0 | 74.1 | 85.1 | 82.3 | 83.5 | 84.4 |
| | CCD_{1000} , fraction of AQX events' area in AQX episodes > 1000×10^4 km ² -days (%) | 34.9 | 18.1 | 15.2 | 70.0 | 53.7 | 23.7 | 51.5 | 46.5 | 49.6 | 39.8 |
| | $\Delta \bar{E}_S$, average increase in E_S for AQX episodes of size S (ppb dec ⁻¹) | 1.7 | 8.3 | 2.9 | 1.5 | 2.4 | 2.0 | 3.9 | 2.3 | 4.6 | 6.9 |

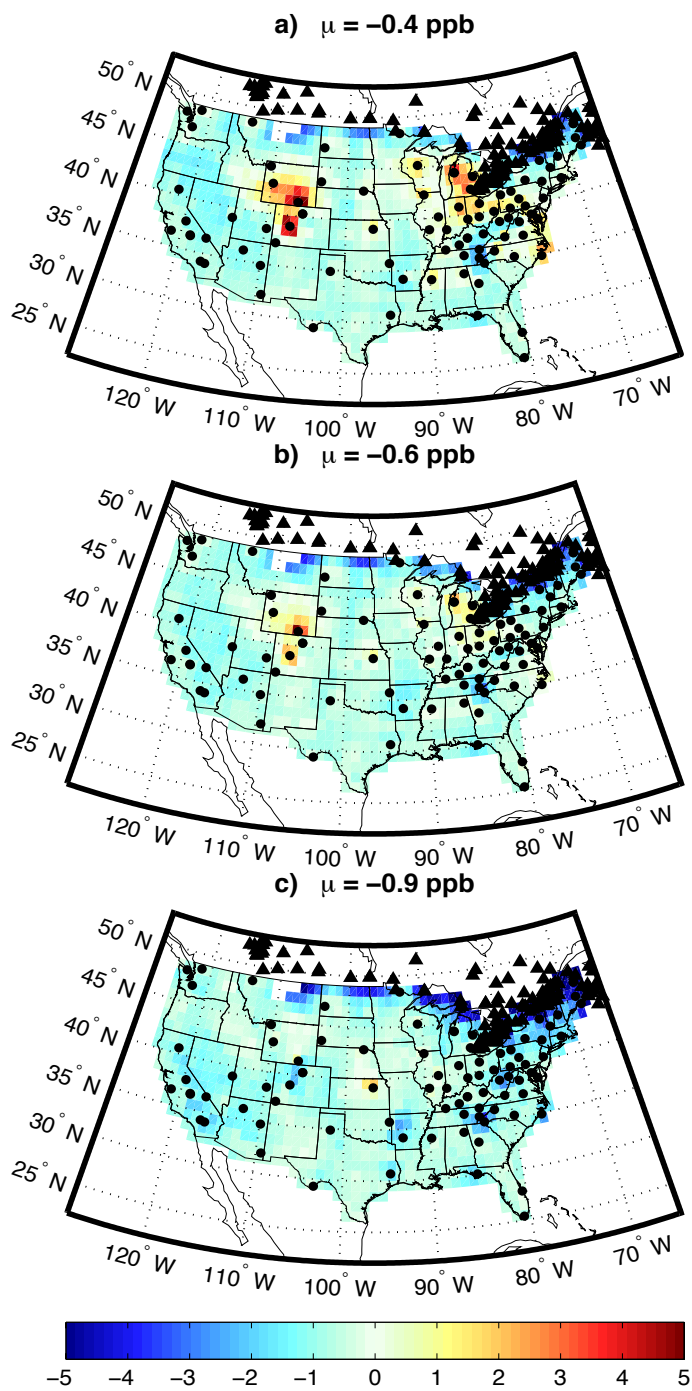


Figure S1. Change in the MDA8 O₃ (ppb) corresponding to the (a) 25th, (b) 50th, and (c) 95th percentiles over NA, shown as the datasets used in this analysis (AQS + CASTNet + NAPS) minus the dataset used in Schnell et al., (2014) (AQS only). The locations of the CASTNet (circles) and NAPS (triangles) stations and the domain area-weighted average difference are shown for each panel.

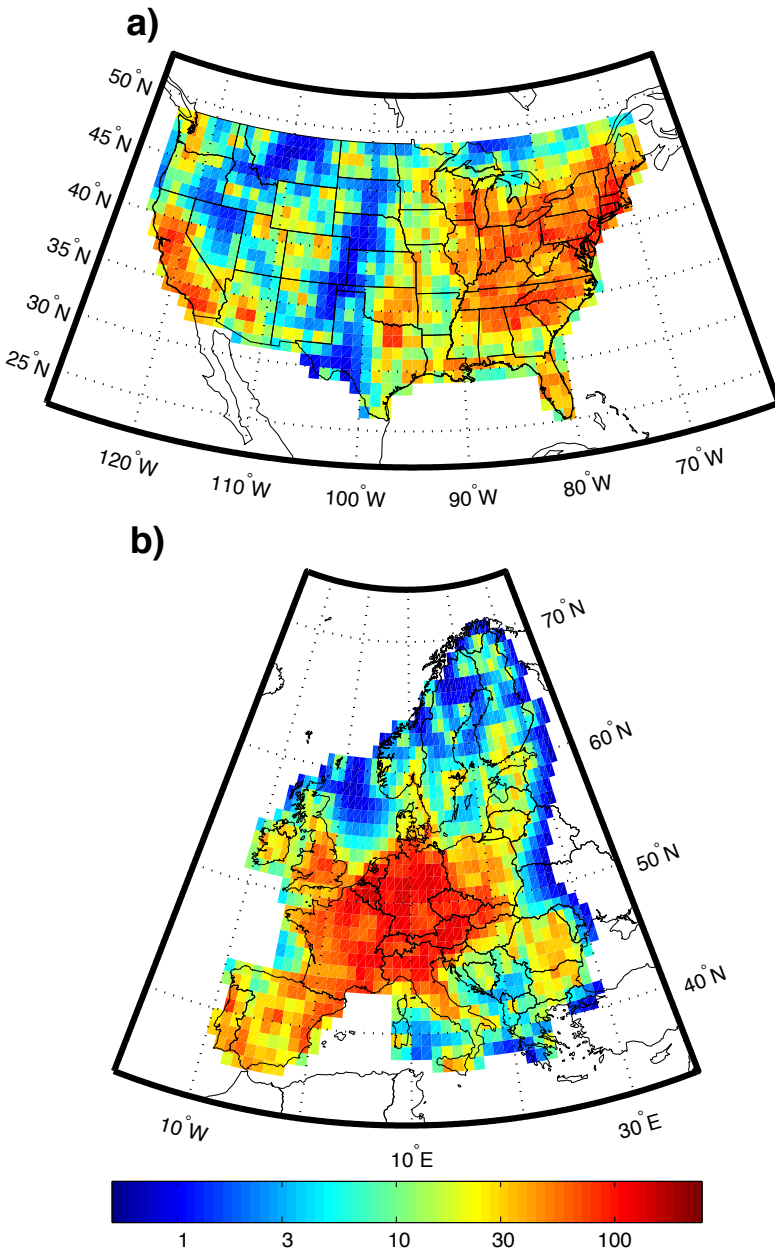


Figure S2. Quality of prediction index (Q^P , see S2014) for the interpolation of the 2000-2009 observations over (a) NA and (b) EU. Note the log-scale of the colorbar.

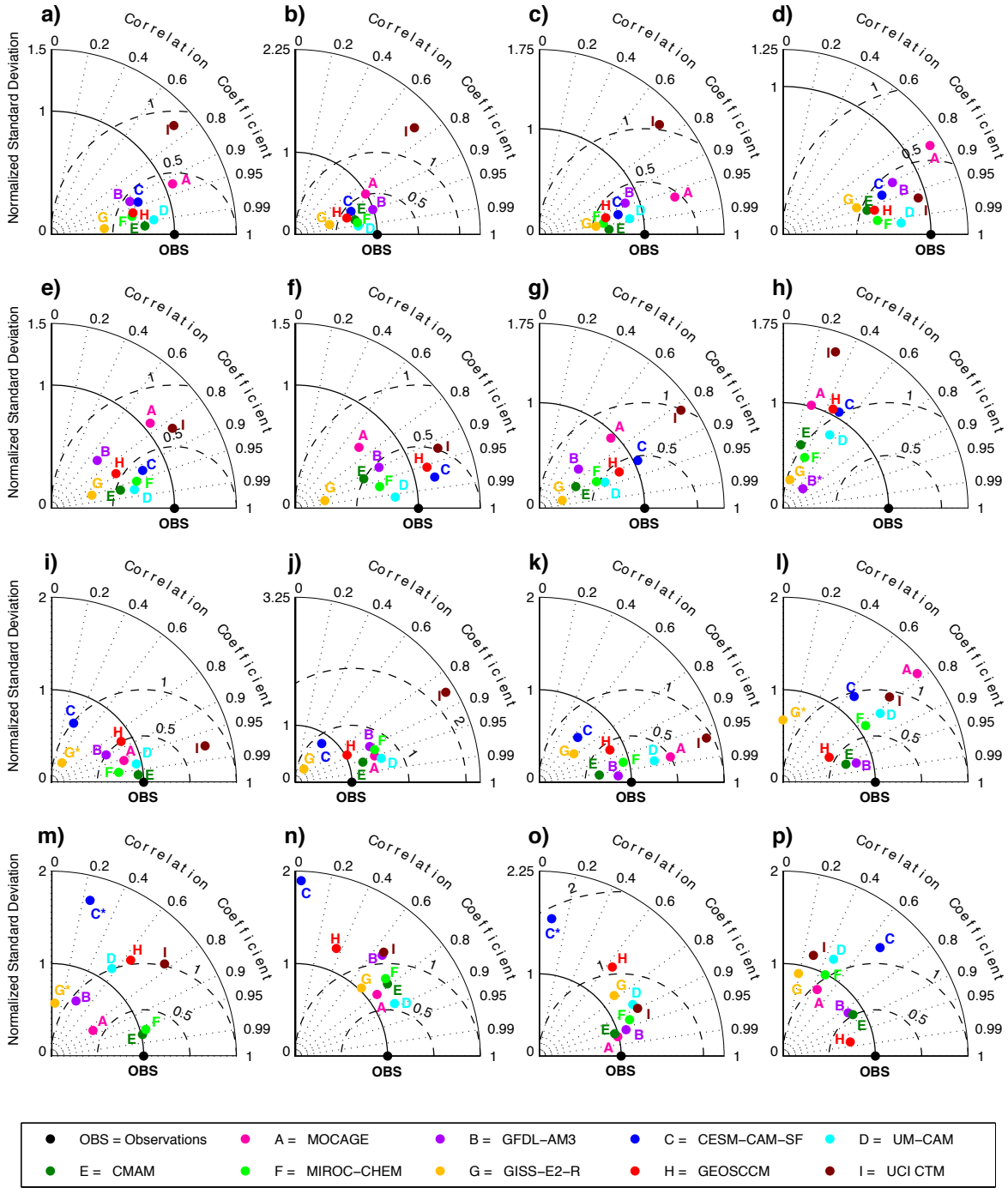


Figure S3. Taylor diagrams comparing the gridded observations of surface O_3 (OBS) to the ACCMIP models (A-H) and the UCI CTM (I) for the (a-d) summer (JJA) diurnal cycle, (e-h) winter (DJF) diurnal cycle, (i-l) annual cycle of MDA8, and (m-p) annual cycle of AQX events averaged over (column 1) WNA, (column 2) ENA, (column 3) SEU, and (column 4) NEU. In cases where a model has a negative correlation, it is plotted as being positive and its letter abbreviation is appended with a “*”.

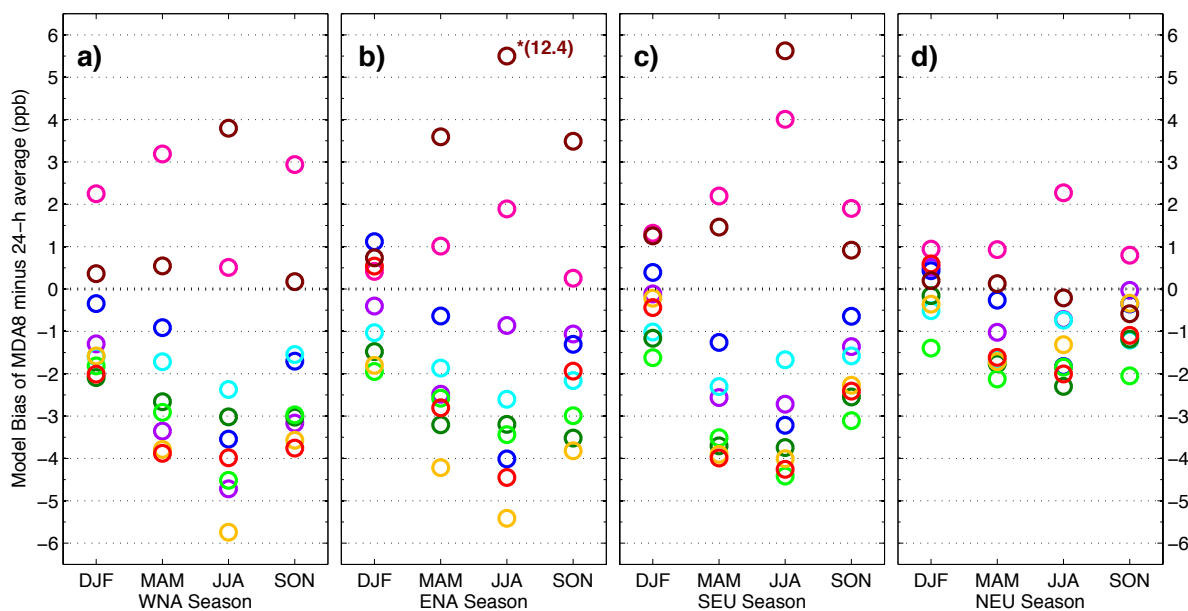


Figure S4. Model biases of MDA8 minus 24 h average O₃ (ppb) in (a) WNA, (b) ENA, (c) SEU, and (d) NEU averaged over winter (DJF), spring (MAM), summer (JJA), and fall (SON). The model corresponding to each colored circle can be found in the legend of Figs. 1 and S3. The circle for model I (dark red) in ENA JJA has been arbitrarily placed since its actual value (12.4 ppb) is outside the range shown in the panel.

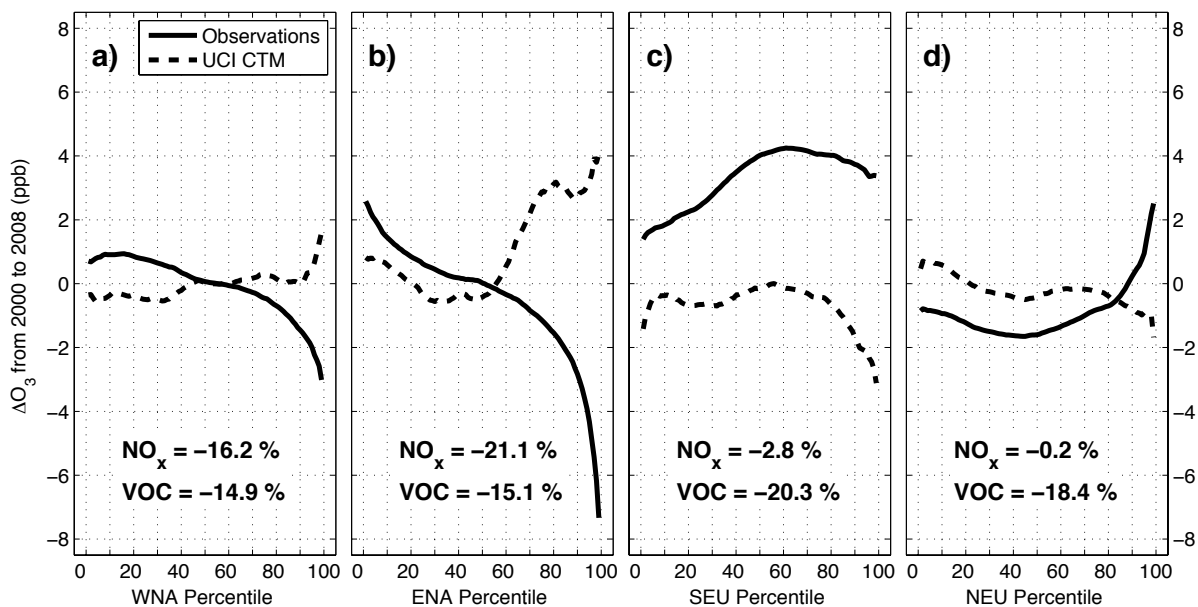


Figure S5. Change in MDA8 O₃ (2008 minus 2000) calculated from a linear fit to the region-wide average MDA8 O₃ corresponding to the 1st to 99th percentiles over (a) WNA, (b) ENA, (c) SEU, and (d) NEU for the observations (solid lines) and UCI CTM (dashed lines). The change (%) in NO_x and total non-methane VOC emissions over the period are also given for each region.

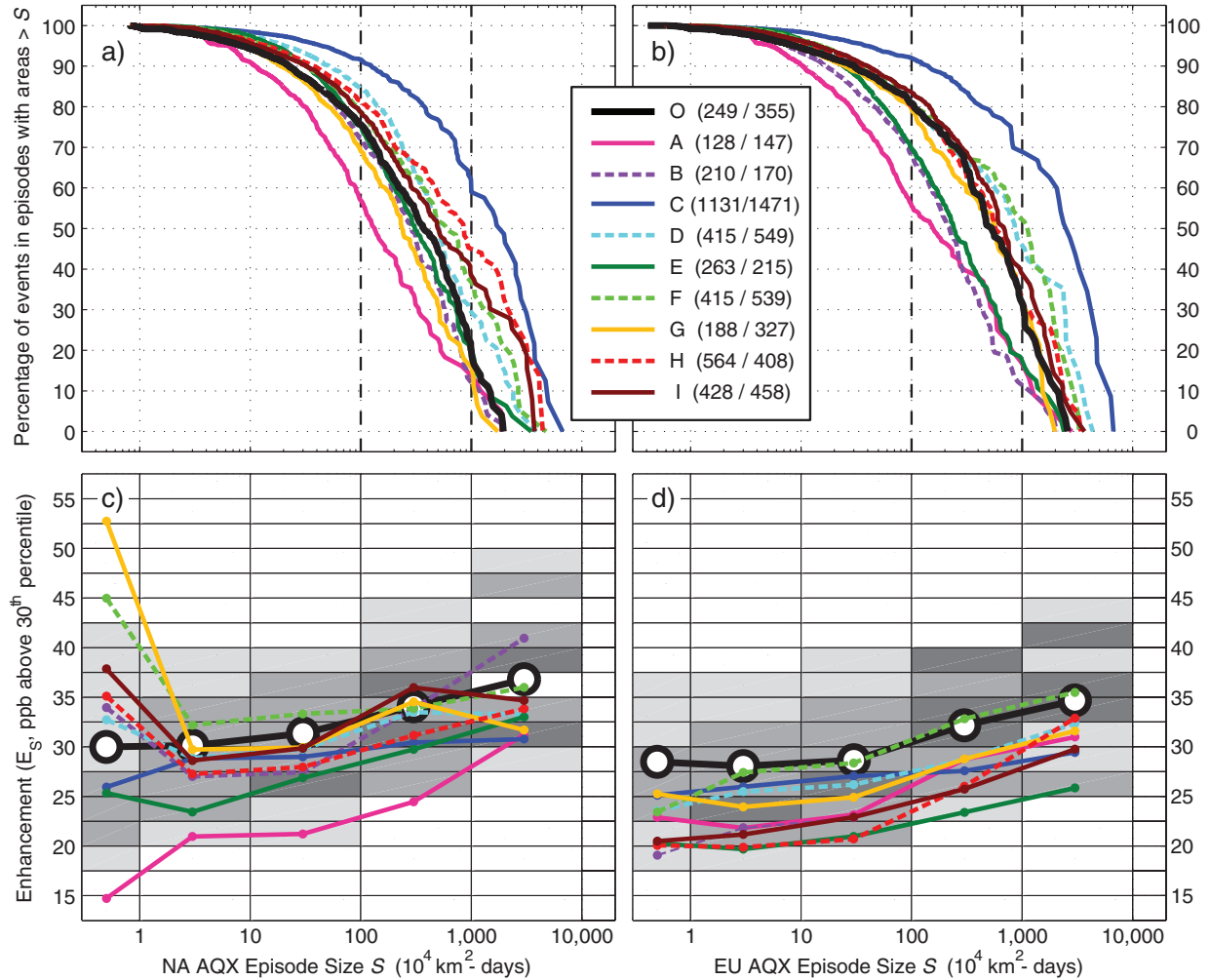


Figure S6. Similar to Fig. 4 but for the 10 AQX events per year case. **(a-b)** Complementary cumulative distribution (CCD) of the percentage of total areal extent of all individual AQX events (10-per-year case) as a function of AQX episode size, (S , $10^4 \text{ km}^2\text{-days}$) for the observations (O), ACCMIP models (A-H), and UCI CTM (I) in **(a)** NA and **(b)** EU. Dashed vertical lines show the graphical representations of CCD_{100} and CCD_{1000} . Mean episode size \bar{S} for each dataset and domain is given in the legend as (NA/EU). **(c-d)** Density scatterplot of the observations enhancement of AQX episodes E_S versus their size S (E_S binned at 5 ppb increments from <15 ppb to >55 ppb, S binned at each log-decade) in **(c)** NA and **(d)** EU. The gray scale represents the relative percentage of AQX episodes in each $(x, y) = (S, E_S)$ bin and includes percent ranges of $\leq 5\%$ (white), 5-10%, 10-15%, and $> 15\%$ (darkest gray) where the size bins (i.e., columns) are normalized to sum to 100%. The overlain curves show the observation's and each model's area-weighted mean enhancement E_S in each size bin. The values of E_S in each size bin for models A and I have been scaled by 0.5 since they are largely outside the range of the others.

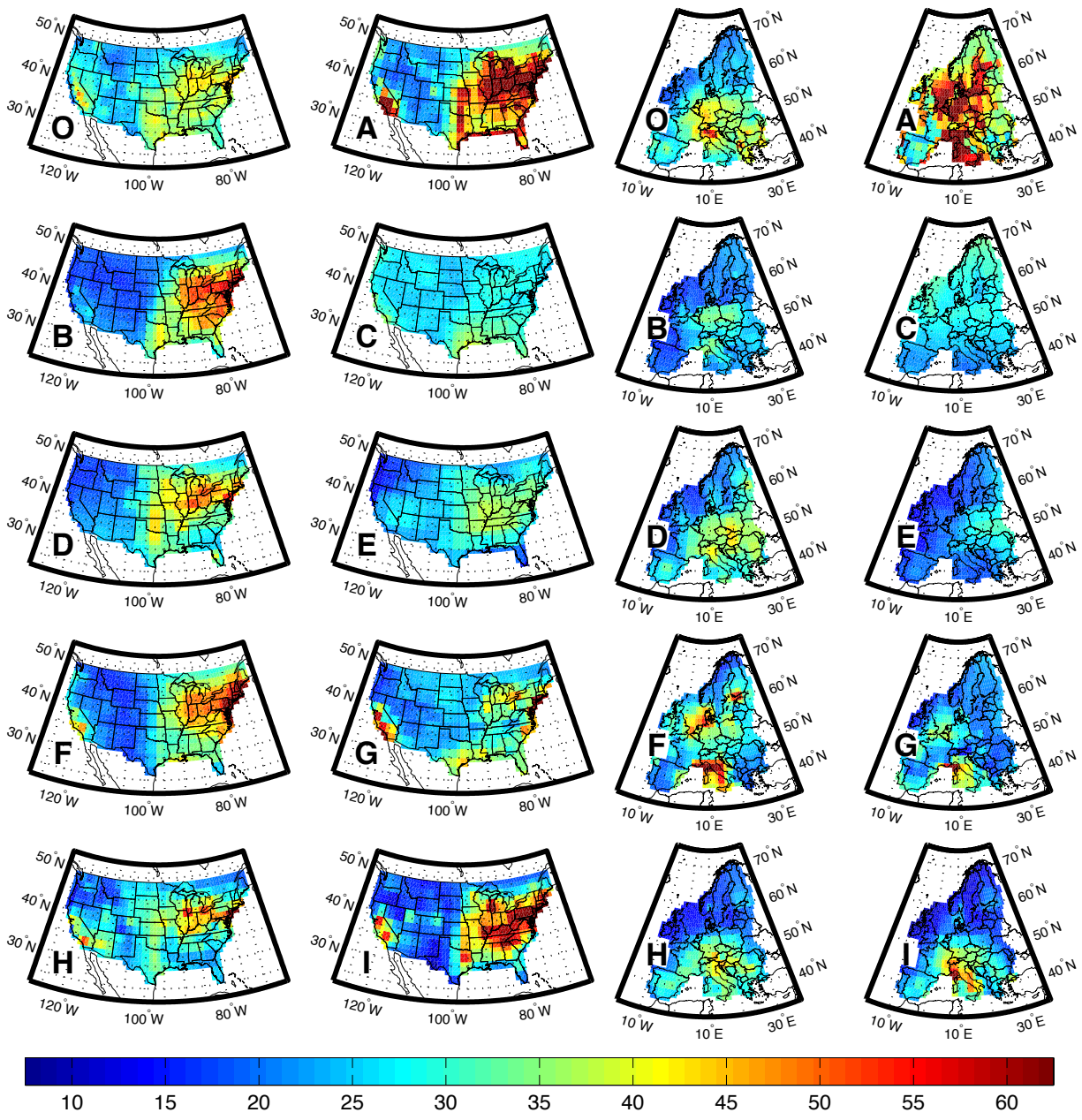


Figure S7. Enhancement at the AQX threshold E_{AQX} = difference between the ~ 97.3 and 30th percentile of the gridded surface MDA8 O₃ (ppb) over (left two columns) NA and (right two columns) EU for the observations (O), ACCMIP models (A-H), and UCI CTM (I). The values of model I are scaled by 0.5 so the same color scale can be used.